

NOVEL MULTISCALE STRUCTURE-BASED MODEL OF THE BOVINE CAUDAL DISC MOTION SEGMENT

Minhao Zhou (1), Grace D. O’Connell (1,2)

(1) Department of Mechanical Engineering
 University of California, Berkeley
 Berkeley, CA, United States

(2) Department of Orthopaedic Surgery
 University of California, San Francisco
 San Francisco, CA, United States

INTRODUCTION

Failure of the annulus fibrosus (AF) due to mechanical overload can accelerate intervertebral disc (IVD) degeneration and cause debilitating pain. Previous studies suggested that fiber mechanics could largely determine AF and thus disc failure behaviors.¹⁻² However, directly measuring *in situ* AF fiber mechanics (*e.g.* fiber stress and strain distributions) is challenging due to experimental limitations and can result in contradicting reported data with large variations.²⁻⁴ Earlier joint-level studies that measured AF fiber strains under physiological axial compressions reported fiber strains that varied considerably from 3 to 55%.³⁻⁵ Thus, despite recent advancement in experimentations, *in situ* AF fiber mechanics at joint level remains poorly understood.

Finite element models have been used to complement experimental studies, providing a powerful tool for predicting hard-to-measure, fiber-reinforced tissue mechanics. However, most IVD models employ homogenization theory and describe every AF element as a combination of fibers and matrix and are thus not capable of explicitly examining subtissue-level mechanics, such as interfibrillar stress and strain distributions.⁶ To address the limitation, we previously developed a multiscale structure-based AF model, where fiber bundles and the extrafibrillar matrix were explicitly modeled to occupy separate volumes. Parameter calibration was conducted at the subtissue level using tissue subcomponent mechanical testing data (*e.g.* fiber bundles and matrix). The model was then validated at tissue level under uniaxial tension, biaxial tension, and shear.⁷⁻⁸ In this study, we will employ this modeling-validation framework to evaluate *in situ* AF fiber mechanics by developing and validating a joint-level model based on discs.

METHODS

We developed the model based on bovine caudal discs using the reported geometry data.⁹ The multiscale structure-based modeling-validation framework used for our tissue-level AF tissue-level models

was employed (**Fig. 1A**).⁷⁻⁸ Gradients in fiber orientation and solid volume fraction from inner to outer AF were described based on literature data (**Fig. 1A–B**).¹⁰ The current model was created at 1:5 scale for computational efficiency; thus, preliminary work was performed to ensure that scaling did not alter model validation results. All model parameters were directly linked to physical or biochemical tissue properties, including modulus, Poisson’s ratio, and fixed charge density (**Fig. 1C**), and were determined based on data in the literature.¹¹⁻¹⁴

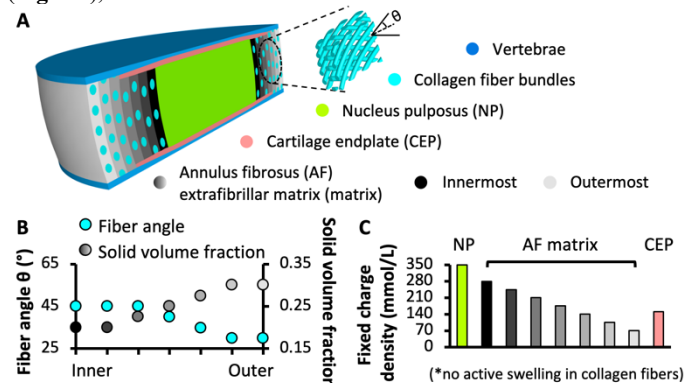


Fig. 1: (A) Disc model at 1:5 scale. (B) Annulus fibrosus structural parameters. (C) Disc fixed charge density distribution.

The model was loaded in two steps: first, the disc was allowed to swell (triphasic) in 0.15 M saline. Intradiscal pressure (IDP) was assessed as the average nucleus pulposus pressure and was compared to human IVD experimental IDP data for validation, due to the lack of IDP data from bovine discs. The second step was one of the three cases: 0.5 MPa axial compression (**Case A**), 10 N·mm axial rotation (**Case B**), or 0.5 MPa axial compression followed by 10 N·mm axial rotation (**Case**

C). Average AF fiber stretch and stress distributions were assessed at 0.5 MPa axial compression for **Case A** and at 10° axial rotation for **Case B** and **C** to represent the higher rotation of bovine discs, where the post-swelling configuration was considered as the reference configuration. Model-predicted compressive and torsional stiffness were normalized by geometry and validated with experimental data.

RESULTS

Across models of three different scales (1:4, 1:5, 1:6), the predicted intradiscal pressure was 0.18 ± 0.006 MPa post-swelling and 0.48 ± 0.006 MPa under 0.5 MPa axial compression. The predicted normalized compressive stiffness was 8.12 ± 0.28 MPa and the predicted normalized torsional stiffness 36 ± 8 kPa°. These model predictions agreed well with literature (Fig. 2). Thus, we considered the current model valid for describing swelling, axial compression and rotation behaviors.

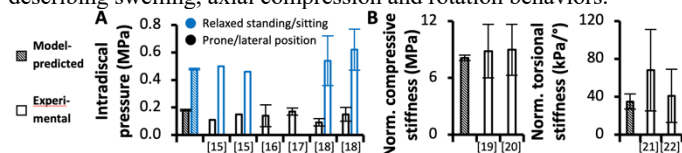


Fig. 2: Model-predicted (A) intradiscal pressure and (B) normalized (norm.) compressive and torsional stiffness vs. experimental data.

Under pure axial compression (**Case A**), the average AF fiber stretch was ~ 1.05 and was consistent throughout the AF (Fig. 3A—black circles). Fiber stretch was comparable under pure rotation (**Case B**), but a linear increase was observed from 1.04 in the innermost AF layer to 1.07 in the outermost layer (Fig. 3A—blue circles). Under combined loading (**Case C**), the average fiber stretch nearly doubled, increasing from ~ 1.05 (**Case A & B**) to ~ 1.10 (Fig. 3A—red circles).

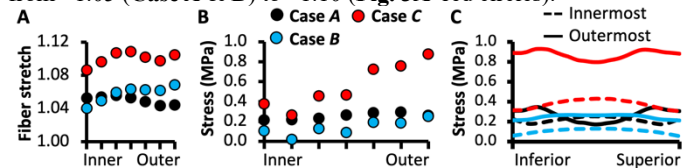


Fig. 3: Average annulus fibrosus (AF) post-loading fiber (A) stretch and (B) stress. (C) AF post-loading fiber stress profiles along the fiber length in the inner- and outermost AF layers.

Strain concentrations were observed near cartilage endplates in inner AF (Fig. 4A). Under pure compression, average AF fiber stress was relatively consistent throughout the AF (0.22–0.29 MPa; Fig. 3B—black circles). The rotation-only loading (**Case B**) reduced fiber stress in the inner-middle AF by $\sim 60\%$ but did not alter the fiber stress in the outer AF (Fig. 3B—blue vs. black circles). Under combined loading (**Case C**), the average fiber stress increased linearly from inner to outer AF, where the combined compression rotation resulted in a more than 1.5-fold increase in inner AF fiber stress and a more than 3-fold increase in the outer AF fiber stress (Fig. 3B—red; Fig. 4).

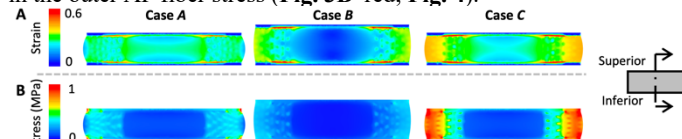


Fig. 4: Post-loading disc (A) strain and (B) stress distributions.

Fiber stress profiles were tracked along the fiber length from the superior to inferior vertebra. In all cases, peak fiber stress was observed near the vertebrae in outer AF (Fig. 3C—solid lines). Pure axial compression or rotation generated comparable fiber stresses across AF. However, the combined loading amplified the difference between outer and inner AF fiber stresses (Fig. 3C—red vs. black & blue lines).

DISCUSSION

The recent shift towards multiscale modeling is important for understanding the IVD subtissue-level degeneration-induced changes

that act to preserve the joint-level properties. Our previous multiscale joint-level model assessed disc swelling behaviors and proved that a computational model developed with parameters directly representing tissue physical or biochemical properties (e.g. fiber modulus or fixed charge density) was capable of replicating morphological changes of degenerated discs, such as the decrease in disc height and the inward bulging of inner AF.²³ This study expanded upon that work by further validating the joint-level mechanics under axial compression and rotation. Additionally, we further expanded the model's capability by modeling AF fiber structure to evaluate fiber mechanics and assess the ability to predict disc failure. Lastly, the multi-scale model-validation framework further expanded our previous tissue and subtissue-level work,⁷⁻⁸ as results of this study proved that the framework is still valid at the joint level, demonstrating its robustness and predictive power.

Physiological disc-joint loadings resulted in a fiber stretch ranging from 1.04 to 1.10, agreeing with previous *in vitro* photogrammetry-based studies,⁴⁻⁵ and indicating a low likelihood of failure based on experimental AF fiber bundle failure stretch data (1.14 ± 0.03).²⁴⁻²⁵ The structure-based modeling technique partially addressed the prior concern about homogeneous models overestimating fiber stretches and thus predicting premature disc failure under physiological loads.⁵ In a previous study, a fiber stretch of ~ 1.13 was observed under physiological axial rotation; the stretch reached up to ~ 1.20 under combined loading configurations, indicating a high likelihood of tissue failure under physiological loading.⁶ We will use the current model to examine more combined loading modalities to strengthen this finding.

Disc failure has been shown to occur through endplate fracture, AF damage in the outer AF, or inward bulging starting from the inner AF. Under all loading conditions, strain concentrations (Fig. 4A) and peak fiber stresses (Fig. 3C) were located near the AF-endplate-vertebrae interfaces, which might help explain the large likelihood of endplate rupture during *in vitro* joint-level tests.²⁶ Interestingly, compared to the pure compression or rotation case, the increase in outer AF stresses result from the combined loading was disproportionately larger than the increase in outer AF strains (Fig. 4). These results agree with observations of AF-only failures that occurred in the outer AF with multiaxial loading applied to ovine lumbar discs.²⁷ Taken together, these findings suggest that disc failure might be driven more by peak stresses than strains, which could serve as an important reference when modeling disc tissue damage.

Concentric and radial annular tears, rim lesions, and annular fissures are common in degenerated discs. Thus, a comprehensive understanding of *in situ* fiber mechanics is essential for predicting AF damage initiation and accumulation, which can be applied to development of workplace loading limits (e.g. factory workers). The modeling framework described here provides a powerful tool for investigating multiscale disc mechanics with degeneration and can be used to develop clinically relevant models that use noninvasive imaging to determine biochemical composition. Ongoing work is leveraging this framework to evaluate changes in biochemical composition on stress distributions between tissues and within tissues to assess how the disc preserves joint-level mechanics during early degeneration.

ACKNOWLEDGEMENTS The work was supported by the National Science Foundation (CMMI: 1760467).

REFERENCES [1] Iatridis+, *JBM*, 2004; [2] Rausch+, *BMMB*, 2016; [3] Shah+, *J Bone Jt Surg*, 1978; [4] Stokes, *JOR*, 1987; [5] Heuer+, *JBM*, 2008; [6] Schmidt+, *Spine*, 2007; [7] Zhou+, *BMMB*, 2020 [8] Zhou+, *JMBBM*, 2021; [9] O'Connell+, *Spine*, 2007; [10] O'Connell+, *BioRes open accs*, 2015; [11] Goel+, *JBME*, 1995; [12] Cortes+, *JBM*, 2014; [13] Bezci+, *JOR Spine*, 2019; [14] Périé+, *JBM*, 2005; [15] Wilke+, *Spine*, 1999; [16] Nguyen+, *J Bone Jt Surg Am*, 2008; [17] Urban+, *Spine*, 1988; [18] Sato+, *Spine*, 1999; [19] Beckstein+, *Spine*, 2008; [20] Bezci+, *JBME*, 2015; [21] Showalter+, *Spine*, 2012; [22] Bezci+, *JMBBM*, 2018; [23] Yang+, *Acta Biomater*, 2020; [24] Skaggs+, *Spine*, 1994; [25] Isaacs+, *JMBBM*, 2005; [26] Adams+, *Spine*, 1985; [27] Berger-Roscher+, *Spine*, 2017